Journal of Photochemistry and Photobiology A: Chemistry 214 (2010) 22–32

Contents lists available at ScienceDirect

Journal of Photochemistry and Photobiology A: Chemistry

journal homepage: www.elsevier.com/locate/jphotochem

Terpyridine- and 2,6-dipyrazinylpyridine-coordinated ruthenium(II) complexes: Synthesis, characterization and application in TiO_2-based dye-sensitized solar cells

Georgios C. Vougioukalakis[a], Thomas Stergiopoulos[a], Georgios Kantonis[a], Athanassios G. Kontos[a], Kyriakos Papadopoulos[a], Arta Stublla[b], Pierre G. Potvin[b], Polycarpos Falaras[a,*]

[a] Institute of Physical Chemistry, NCSR "Demokritos", Agia Paraskevi Attikis, 15310 Athens, Greece
[b] Department of Chemistry, York University, 4700 Keele Street, Toronto, ON, M3J 1P3, Canada

ARTICLE INFO

Article history:
Received 16 March 2010
Received in revised form 11 May 2010
Accepted 1 June 2010
Available online 8 June 2010

Keywords:
Dye-sensitized solar cells
Dyes
Ruthenium
TiO_2

ABSTRACT

Two new ruthenium(II) complexes bearing terpyridine- or 2,6-dipyrazinylpyridine ligands have been prepared and characterized by one- and two-dimensional NMR techniques, ESI mass spectrometry, as well as by UV–vis, emission, FTIR, Raman, and cyclic voltammetry studies. The structure of the terpyridine-coordinated complex resembles that of black dye (tris(thiocyanato)(2,2′:6′,2″-terpyridyl-4,4′,4″-tricarboxylato)ruthenium(II) tris(tetra butylammonium) salt), while the spectral data of the 2,6-dipyrazinylpyridine-coordinated complex are consistent with an unanticipated, unsymmetrical binuclear structure. The ruthenium(II)/(III) oxidation potential of the terpyridine-coordinated dye was measured at +0.87 V (vs. Ag/AgCl), about 200 mV higher than the oxidation potential of black dye. According to a series of desorption experiments, both new dyes were found to adsorb on TiO_2 to a greater extent than black dye. The photo-electrochemical properties of both dyes were investigated and compared to that of black dye; while the 2,6-dipyrazinylpyridine-coordinated complex was found to be a very poor sensitizer, the cells obtained from the terpyridine-coordinated dye show power-conversion efficiencies which are more than half of that attained by black dye. Finally, preliminary electron dynamics studies of the cells constructed with the terpyridine dye were carried out and the results are compared to that of black dye cells.

1. Introduction

The development of renewable, non-polluting power resources has become an extremely important need in view of fossil fuels depletion, increasing world energy consumption, and concerns over global environment preservation and climate change [1,2]. One of the most interesting and promising strategies seeking to tackle this problem is to mimic nature in harvesting and collecting sunlight, thus attaining clean and affordable solar electricity [3,4]. Indeed, solid-state photovoltaic cells, based on inorganic semiconductors, have proven to achieve this goal; however, their high production cost imposes restrictions on their mass utilization [5,6]. Dye-sensitized solar cells (DSSCs) constitute an appealing alternative to the classical solid-state cells [7–15]. DSSCs are based on nanocrystalline metal oxide semiconductors, sensitized by molecular dyes (sensitizers) that promote photoinduced charge separation [16,17]. The system is basically comprised of two facing electrodes: a transparent photoanode, consisting of a thin nanoparticulate film (7–20 μm) of a mesoporous semiconductor oxide modified with a monolayer of sensitizer molecules, which are chemically grafted via functional groups such as –COOH and $-PO(OH)_2$, and a Pt counter electrode, both deposited on conductive glass substrates. An appropriate medium containing the redox couple (usually I^-/I_3^-) is placed between the two electrodes to transfer the charges.

The photo-electrochemical cycle in DSSCs begins when a dye molecule undergoes transition into its excited state via light absorption. The photoexcited dye molecule subsequently injects an electron into the conduction band of the semiconductor. Ideally, the photoinjected electron percolates through the nanoparticle network, gets collected by the photoanode electrode, and then travels through the external circuit performing electrical work. The electron eventually reaches the counter electrode and reduces the electron mediator species, generating the reducing agent that concomitantly reduces the ground state oxidized dye, completing the circuit. The device maximum voltage (V_{max}) that can be generated equals the difference between the semiconductor Fermi level and the electron mediator species' (i.e. I^-/I_3^-) redox potential. Overall, the device results in the conversion of photons to electrons, while no chemical species are consumed nor transformed.

* Corresponding author. Tel.: +30 210 6503644; fax: +30 210 6511766.
E-mail address: papi@chem.demokritos.gr (P. Falaras).

1010-6030/$ – see front matter © 2010 Elsevier B.V. All rights reserved.
doi:10.1016/j.jphotochem.2010.06.001

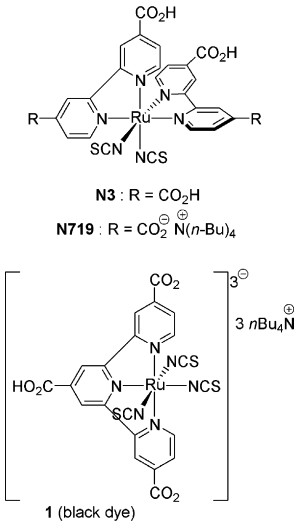

Fig. 1. Molecular structures of ruthenium(II) dyes **N3**, **N719**, and black dye (**1**).

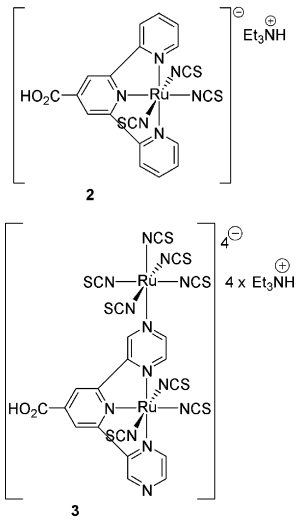

Fig. 2. Molecular structures of the new terpyridine- and 2,6-dipyrazinylpyridine-coordinated ruthenium(II) dyes (**2**) and (**3**).

The efficiency of a DSSC largely depends on the charge generation step and, therefore, the sensitizer utilized. Some of the requirements that an efficient sensitizer has to fulfill include [7–14]: (i) a broad and strong absorption, preferably extending from the visible to the near-infrared; (ii) a firm, irreversible adsorption to the semiconductor's surface and a strong electronic coupling between its excited state and the semiconductor conduction band; (iii) chemical stability in the ground as well as in the excited and oxidized states; (iv) a reduction potential sufficiently higher (by ~150–200 mV [18]) than the semiconductor conduction band edge in order to bring about an effective electron injection; and (v) an oxidation potential sufficiently lower (by ~200–300 mV [18]) than the redox potential of the electron mediator species, so that it can be regenerated rapidly.

A variety of organic dyes and transition-metal complexes has been successfully employed as sensitizers in DSSCs thus far [19–24]; in terms of photovoltaic performance and long-term stability, Ru(II) polypyridyl complexes comprise the most successful family of DSSCs sensitizers [25–29]. The first high-performance Ru(II) sensitizer was reported in 1993 by Grätzel and co-workers (**N3** and **N719**, Fig. 1) [30,31]. In 1997, the same group published the synthesis and evaluation of a terpyridyl analogue, i.e. "black dye" (**1**, Fig. 1) [32,33]. The reported overall power-conversion efficiencies of **N3**, **N719**, and black dye are 10.0%, 11.2%, and 10.4%, respectively. Since then, a series of modifications of these early Ru(II) complexes have, among others, led to sensitizers with amphiphilic properties and/or extended conjugation, achieving power-conversion efficiencies up to 11.9% [34,35].

In this kind of ruthenium sensitizers, the stereoelectronic characteristics of the polypyridine ligand along with the number of functional binding groups are of high importance for efficient sensitization. As part of our ongoing work in the field of DSSCs [36–40], we herein report the synthesis, characterization, and TiO_2-sensitizing ability evaluation of two new Ru(II) dye complexes, coordinated with terpyridine (**2**) and 2,6-dipyrazinylpyridine (**3**) ligands (Fig. 2). Both ligands encompass one peripheral carboxylic anchoring group; furthermore, the 2,6-dipyrazinylpyridine moiety is more electron-withdrawing than the terpyridine one, due to the additional nitrogen atoms contained in the framework of the former. Comparison of sensitizers such as (**2**) and (**3**) with black dye (**1**) provides more insight into the sensitizers optimum structure and geometry, paving the way for a more detailed structure–function correlation in these systems.

2. Experimental

2.1. Materials and methods

Unless otherwise stated, all reagents were purchased from Aldrich. Solvents were purchased from Fluka or Panreac and used without further purification. Trihydrated ruthenium(III) trichloride was purchased from Riedel-de Haën. Acetonitrile, used in the electrochemical studies, was degassed by a freeze–pump–thaw cycle and stirred overnight over P_2O_5, at room temperature, under an argon atmosphere. It was then distilled under argon and degassed again via another freeze–pump–thaw cycle, before being stored over activated 4 Å molecular sieves. All synthetic reactions were performed under an argon atmosphere in degassed (15 min of argon bubbling) solvents. Black dye (tris(thiocyanato)(2,2′:6′,2″-terpyridyl-4,4′,4″-tricarboxylato)ruthenium(II) tris(tetrabutylammonium) salt) was purchased from Solaronix.

2.1.1. Analytical measurements

^1H, ^{13}C, HSQC, and COSY Nuclear Magnetic Resonance (NMR) spectra were obtained with a Bruker Avance 500 MHz spectrometer in $(CD_3)_2SO$ or CD_3OD. Chemical shifts are reported in ppm downfield from Me_4Si, by using the residual solvent peak as internal standard. Data for NMR spectra are reported as follows: chemical shift (δ ppm), multiplicity, coupling constant (Hz), and integration. Electronic spectra (UV–vis) in solution (**1**: 5.01×10^{-5} M; **2**: 5.62×10^{-5} M; and **3**: 3.44×10^{-5} M in DMF) were recorded with a Hitachi 3010 spectrophotometer. Diffuse reflectance and transmittance UV–vis spectra of the dye-sensitized TiO_2 films were obtained on the same instrument using an integrating sphere with 60 mm diameter. Emission spectra (**2**: 9.04×10^{-5} M in DMF) were recorded on a JASCO FP 777 spectrophotometer. Infrared spectra (FTIR) in the powder form were obtained using a FTIR Nicolet 6700 spectrometer. Data for FTIR spectra are reported as follows: frequency (cm^{-1}) and strength (s = strong; m = medium; w = weak). Despite our repeated attempts, we were unable to get reliable Elemental Analysis data for any of the newly synthesized complexes, possibly due to insufficient combustion. Micro-Raman spectra were measured in the backscattering configuration using a Renishaw inVia spectrometer with an Ar^+ ion laser (λ = 514.5 nm) and a near-infrared (NIR) diode laser (λ = 785 nm), as excitation sources. In all cases, very low laser power density (0.05 mW/μm^2) was applied to avoid dye degradation and thermal shifts of the modes. Cyclic

voltammetry measurements were performed in 10^{-3} M solutions of the corresponding complexes in acetonitrile containing 0.1 M tetrabutylammonium tetrafluoroborate (TBATFB) as supporting electrolyte, at a sweep rate of 100 mV/s, using the Autolab PGSTAT-30 potentiostat (Ecochemie). A three-electrode one-compartment electrochemical cell was used, with Metrohm dot (6.0302.000) and planar (6.0305.000) platinum working and counter electrodes, respectively, as well as a Metrohm Ag/AgCl 6.0726.100 reference electrode (LiCl saturated in ethanol). The experiments were performed in deoxygenated solutions purified by Ar gas (99.9%) for 30 min prior to use. During the experiments Ar was passing over the solution surface. Electrospray Ionization Mass spectra (ESI/MS) were recorded using an AQA Navigator, Finnigan Mass Spectrometer. Accurate mass measurements were obtained on solutions in CH_3OH-CH_2Cl_2 with an AB/Sciex QStar mass spectrometer with an ESI source in either positive or negative ion mode and Time of Flight detection.

2.1.2. Crystal structure determination

Crystals of ethyl 2,6-dipyrazin-2-ylisonicotinate were obtained from $CHCl_3$ by slow evaporation, and analyzed by Dr. A. Lough (University of Toronto). X-ray diffraction data were collected on a Bruker-Nonius Kappa-CCD diffractometer using monochromated Mo Kα radiation and were measured using a combination of *f* scans and *w* scans with *k* offsets, to fill the Ewald sphere. The data were processed using the Denzo-SMN package. Absorption corrections were carried out using SORTAV. The structure was solved and refined using SHELXTL V6.1 for full-matrix least-squares refinement that was based on F^2. All H atoms were included in calculated positions and allowed to refine in riding-motion approximation with U_{iso} tied to the carrier atom. Crystallographic data: formula $C_{16}H_{13}N_5O_2$; Fw 307.31; *T* 150(2) K; triclinic space group $P\bar{1}$ (#2); lattice constants: *a* 101.013(2) Å, *b* 9.6459(5) Å, *c* 19.6025(9) Å; α 101.013(2)°, β 91.151(3)°, γ 100.872(3)°, *V* 696.97(5) Å^3; *Z* 2; D_{calc} 1.464 Mg/m^3; μ 0.102 mm^{-1}; λ(Mo Kα) 0.71073 Å; $2\theta_{max}$ 27.49°; 3117 independent reflections measured (R_{int} 0.0333), of which 2336 were considered to be observed with $I > 2\sigma(I)$; max. residual electron density 0.300 and −0.295 e/Å^{-3}; 209 parameters (the position of the H atoms were calculated at idealized positions); R_1 0.0495; wR_2 0.1458. Crystallographic data have been deposited at the Cambridge Crystallographic Data Centre, 12 Union Road, Cambridge CB2 1EZ, U.K., and copies can be obtained on request, free of charge, by quoting the publication citation and the deposition number 7757703, or via www.ccdc.cam.ac.uk/data_request/cif.

2.1.3. Device assembly

Titania films were prepared using the doctor-blade technique by depositing three different layers of TiO_2 on a 6 mm transparent conductive glass (fluorine-doped tin oxide, FTO) provided with an antireflective coating (Activ Clear, Pilkington). The first layer was prepared from a paste of nanocrystalline powder (Degussa P25) dispersed in distilled water, following a standard experimental procedure [30]. The films were then heated at 120 °C for 30 min. A second layer was deposited on top of the former films by doctor-blading a paste of large scattering particles (Ti-Nanoxide 300, Solaronix), mixed with Degussa P25 in order to improve the films' adherence. Afterwards, the films were thermally treated at 550 °C for 1 h. Finally, a third, very thin layer was added through a simple immersion of the as-annealed films in an aqueous solution of $TiCl_4$. The films were then thoroughly cleaned with water and ethanol and re-annealed at 550 °C. The final thickness of the resultant films (22 μm) was measured by a profilometer. The thermally treated titania films were sensitized by overnight immersion in 0.3 mM ethanolic dye solutions. In order to evaluate their photovoltaic performance, the dye-sensitized films were incorporated as the active photoelectrode (PE) in a lamellar solar cell configuration of the following structure: conductive glass/TiO_2 + dye/electrolyte/Pt/TEC15. TEC15 conductive glasses (Pilkington), platinized by sputtering (about 10 nm thick), were used as counter electrodes (CE). Non-sealed DSSCs were fabricated by placing a drop of an ionic salt-based liquid electrolyte (PMII, Dyesol Ltd.) onto the photoelectrode and sandwiching the CE on top of the PE.

2.1.4. Photo-electrochemical measurements

Current–voltage (*I–V*) measurements were performed by illuminating the DSSCs using solar-simulated light (1 sun, 1000 W/m^2), from a 300 W Xe lamp, in combination with AM 1.5G and UV optical filters (Oriel). The active area of the DSSCs was set at 0.152 cm^2, using a black metallic mask in front of the cell (while the aperture area was larger, 0.360 cm^2). *I–V* characteristics were obtained using linear sweep voltammetry (scan speed: 50 mV/s) on an Autolab PGSTAT-30 potentiostat. Electron diffusion coefficients and lifetimes were determined by intensity-modulated photocurrent spectroscopy (IMPS) and intensity-modulated voltage spectroscopy (IMVS), respectively. A red light (625 nm) emitting diode was used as the light source for both AC and DC illumination controlled by the FRA module. The LED intensity, calibrated by a Si photodiode (Thorlabs), was varied using neutral optical filters.

2.2. Synthesis

2.2.1. Synthesis of Ethyl 2,2′:6′,2″-terpyridine-4′-carboxylate

2-Acetylpyridine (290 mg, 2.4 mmol, 2 equiv.) and ethyl glyoxalate (0.238 mL, 1.2 mmol, 1 equiv.) were dissolved in CH_3OH (8 mL) by stirring for 5 min, followed by addition of 15% KOH (7.2 mL) and conc. NH_4OH (0.8 mL). The mixture was allowed to stand at ambient temperature for 3 days. The emulsion formed was filtered off and washed with $CHCl_3$ (4 mL) and cold 1:1 CH_3OH:H_2O (4 mL). The crude product was suspended in CH_3OH:H_2O (80:20) and the mixture was stirred and sonicated at 35 °C until a clear solution was obtained. This was then acidified to pH 2, by addition of 1 M HCl, to give a suspension that was collected by filtration and carefully washed with a small amount of slightly acidified water and a small amount of cold water. After drying under vacuum, the crude K^+/NH_4^+ salt was dissolved in EtOH in the presence of a catalytic amount of H_2SO_4 and heated to reflux for 2.5–3 days. The pure product was isolated as white flakes after extraction with CH_2Cl_2 (yield 54%). ^{1}H NMR ($CDCl_3$, 400 MHz): δ 1.48 (t, 3H), 4.50 (q, 2H), 7.38 (dd, 2H), 7.89 (dd, 2H), 8.67 (d, 2H), 8.76 (d, 2H), 9.00 (s, 2H). $^{13}C\{^1H\}$ NMR ($CDCl_3$, 100 MHz): δ 14.3, 61.8, 120.5, 121.2, 124.1, 136.9, 140.1, 149.3, 155.4, 156.4, 165.3. Anal. Found for $C_{18}H_{15}N_3O_2$: C, 70.81; H, 5.05; N, 13.43. Calcd: C, 70.8; H, 4.95; N, 13.76. EI-MS: *m*/*z* 305 (43%), 276 (3%), 260 (6%), 233 (100%). FTIR ν_{max} (cm^{-1}) 1725 (C=O str).

2.2.2. Synthesis of [Ru(ethyl 2,2′:6′,2″-terpyridine-4′-carboxylate)Cl_3] (**4**)

A two-necked, 50 mL round-bottomed flask, equipped with a stirring bar and a reflux condenser, was charged with $RuCl_3 \cdot 3H_2O$ (130.7 mg, 0.5 mmol, 1 equiv.) and degassed EtOH (14 mL) at room temperature under argon. The ligand ethyl 2,2′:6′,2″-terpyridine-4′-carboxylate (152.7 mg, 0.5 mmol, 1 equiv.) was dissolved in degassed CH_2Cl_2 (14 mL) and added to this solution. The reaction mixture was refluxed in the dark under argon, for three and a half hours, before let to cool down to ambient temperature. This deep red solution was left overnight at room temperature under argon, in the dark, then filtered on a G4 sintered glass crucible, and washed thoroughly with EtOH (5 × 5 mL) and Et_2O (5 × 5 mL). The remaining dark brown powder was dried overnight under high vacuum (210.0 mg, 82%). FTIR ν_{max} (cm^{-1}) 1720.2 (s), 1600.6 (m), 1552.4

(w), 1463.7 (w), 1419.4 (s), 1365.4 (m), 1346.1 (w), 1257.4 (s), 1245.8 (s), 1162.9 (w), 1118.5 (m), 1012.5 (m), 912.2 (w), 865.9 (w), 794.5 (s), 765.6 (s), 725.1 (s), 651.8 (w), 433.9 (m). ESI/MS (+ mode): m/z 495.0 ($[M–Cl+H_2O]^+$, 40%), 477.0 ($[M–Cl]^+$, 21%), 305.1 ($[L+H]^+$, 30%). Exact mass calculated for $C_{18}H_{17}N_3O_3Cl_2Ru$ $[M–Cl+H_2O]^+$ 494.9684, observed 494.9665.

2.2.3. Synthesis of {$(CH_3CH_2)_3NH$}[Ru(2,2′:6′,2″-terpyridine-4′-carboxylic acid)$(NCS)_3$] (**2**)

A two-necked, 50 mL round-bottomed flask, equipped with a stirring bar and a reflux condenser, was charged with **4** (154.5 mg, 0.3 mmol, 1 equiv.) and degassed DMF (9.3 mL) at room temperature under argon. NH_4NCS (730.8 mg, 9.6 mmol, 32 equiv.) was dissolved in degassed H_2O (3.6 mL) and added to this solution. The reaction mixture was heated at 135 °C in the dark under argon for 45 min. Next, degassed H_2O (5.4 mL) and Et_3N (10.8 mL) were added, and the solution was refluxed (135 °C) for 20 more hours to hydrolyze the ester functionality. The reaction mixture was cooled down to room temperature and the solvent volume was reduced to about 0.5 mL on a rotary evaporator. H_2O (15 mL) was then added, causing a dark brown powder to precipitate. This was washed thoroughly (on a G4 sintered glass crucible) with H_2O (6 × 5 mL) and Et_2O (6 × 5 mL), redissolved in the minimum amount of DMF, precipitated with MeOH, and washed on a G4 sintered glass crucible with Et_2O (3 × 5 mL), to afford complex **2** as a black powder that was dried overnight under high vacuum (137.5 mg, 70%). ^{1}H NMR (CD_3OD, 500 MHz – due to peak overlap only the major isomer's data are given): δ 8.99 (d, J = 4.9 Hz, 2H), 8.76 (s, 2H), 8.48 (d, J = 7.9 Hz, 2H), 8.03 (t, J = 7.6 Hz, 2H), 7.71 (t, J = 6.5 Hz, 2H), 3.21 (q, J = 7.3 Hz, 6H), 1.30 (t, J = 7.3 Hz, 9H). $^{13}C\{^1H\}$ NMR (CD_3OD, 125 MHz): 167.33, 162.72, 160.21, 154.57, 138.01, 137.58, 134.32, 129.45, 128.41, 123.89, 121.64, 48.11, 9.36. FTIR ν_{max} (cm^{-1}) 2104.0 (s), 1693.2 (m), 1596.8 (m), 1471.4 (w), 1421.3 (m), 1336.4 (m), 1276.7 (m), 1234.2 (m), 1155.2 (w), 1041.4 (m), 1014.4 (w), 892.9 (w), 881.3 (w), 790.7 (m), 763.7 (s), 727.0 (m), 651.8 (w), 528.4 (m). ESI/MS (– mode): m/z 552.9 ($[M]^-$, 100%), 493.9 ($[M–H–NCS]^-$, 26%). Exact mass calculated for $C_{19}H_{11}N_6O_2S_3Ru$ $[M]^-$ 552.9154, observed 552.9160. ESI/MS (– mode): m/z 553.3 ($[M]^-$, 100%).

2.2.4. Synthesis of 4-Ethyl 2,6-dipyrazin-2-ylisonicotinate

Using 2-acetylpyrazine (295 mg, 2.4 mmol) instead of 2-acetylpyridine, this was prepared in exactly the same fashion as was ethyl 2,2′:6′,2″-terpyridine-4′-carboxylate (yield 54%). ^{1}H NMR ($CDCl_3$, 400 MHz): δ 1.50 (t, 3H), 4.53 (q, 2H), 8.70 (d, 2H), 8.72 (d, 2H), 9.02 (s, 2H) 9.85 (s, 2H). $^{13}C\{^1H\}$ NMR ($CDCl_3$, 100 MHz): 14.3, 62.1, 121.4, 140.6, 143.4, 143.8, 145.0, 150.1, 155.0, 164.7. Anal. Found for $C_{16}H_{13}N_5O_2$: C, 62.55; H, 4.25; N, 22.64. Calcd: C, 62.53; H, 4.26; N, 22.79. EI-MS: m/z 307.19 (97%), 279.17 (8%), 262.15 (7%), 235.15 (100%). FTIR ν_{max} (cm^{-1}) 1720 (C=O str).

2.2.5. Synthesis of [Ru(ethyl 2,6-dipyrazin-2-ylisonicotinate)Cl_3] (**5**)

This complex was prepared and purified as described for complex **4** (86% yield). FTIR ν_{max} (cm^{-1}) 1722.1 (s), 1583.3 (m), 1562.1 (w), 1467.6 (w), 1375.0 (s), 1346.1 (w), 1243.9 (s), 1168.7 (w), 1118.5 (m), 1091.5 (w), 1020.2 (m), 910.2 (s), 850.5 (w), 771.4 (m), 688.5 (m), 651.8 (w), 615.2 (w). ESI/MS (+ mode): m/z 497.0 ($[M–Cl+H_2O]^+$, 7%), 479.0 ($[M–Cl]^+$, 4%), 442.0 ($[M–OEt–Cl+H_2O]^+$, 3%), 330.1 ($[L+Na]^+$, 7%), 308.1 ($[L+H]^+$, 100%). Exact mass calculated for $C_{16}H_{15}N_5O_3C_{12}Ru$ $[M–Cl+H_2O]^+$ 496.9589, observed 496.9606.

2.2.6. Synthesis of {$(CH_3CH_2)_3NH$}$_4$[Ru$(NCS)_3$(2,6-dipyrazin-2-ylisonicotinic acid)Ru$(NCS)_5$] (**3**)

This complex was prepared and purified as described for complex **2** (88% yield). ^{1}H NMR (CD_3OD, 500 MHz): δ 10.78 (s, 1H), 10.57 (s, 1H), 9.40 (s, 1H), 9.26 (s, 1H), 9.13 (s, 1H), 9.07 (s, 1H), 8.77 (s, 1H), 8.74 (s, 1H), 3.27 (q, J = 7.2 Hz, 24H), 1.35 (t, J = 7.2 Hz, 36H). $^{13}C\{^1H\}$ NMR (CD_3OD, 125 MHz): 164.73, 162.61, 162.47, 152.41, 152.24, 150.42, 150.22, 149.95, 148.95, 147.62, 141.62, 141.16, 140.93, 119.39, 118.94, 118.46, 118.37, 45.40, 6.59. FTIR ν_{max} (cm^{-1}) 2098.2 (s), 1716.4 (w), 1571.7 (s), 1467.6 (w), 1446.4 (w), 1371.2 (s), 1240.0 (w), 1178.3 (w), 1157.1 (w), 1116.6 (w), 1054.9 (w), 1016.3 (w), 904.5 (w), 848.5 (w), 788.8 (m), 775.3 (m), 688.5 (w), 648.0 (s), 455.1 (w).

3. Results and discussion

3.1. Synthesis, NMR, and MS studies of ruthenium dyes

The synthesis of ethyl 2,2′:6′,2″-terpyridine-4′-carboxylate has been reported in the literature [41–47] but it and the completely new ethyl 2,6-dipyrazin-2-ylisonicotinate were prepared by a new method, both in 54% yields, from commercial materials, and both were fully characterized. Fig. 3 reports the crystal structure for the latter ligand. As is typical for tridentates, exemplified by the 4-p-tolyl analogue [48], the pyrazine rings are rotated out of the metal-binding conformation to minimize dipole–dipole repulsions. The ethyl ester group is twisted out of coplanarity with the pyridine ring by 15.5°, although this may simply be to facilitate the packing of the ethyl groups in the voids between stacks of tridentate moieties.

Complex **2** was prepared via the two-step synthetic route presented in Scheme 1, in 57% total isolated yield, following a modification of previously reported procedures [32,33]. All reactions were monitored by removing small aliquots, which were subsequently analyzed via UV–vis and ^{1}H NMR spectroscopy. Complex **2** was characterized by ^{1}H, ^{13}C, COSY, and HSQC NMR experiments, UV–vis and FTIR spectroscopy (vide infra), as well as ESI-TOF and ESI mass spectrometry. Also, it has to be noted that, despite our repeated attempts, we were unable to isolate and purify the carboxylic analogue of complex **4** via the reaction of $RuCl_3 \cdot 3H_2O$ with 2,2′:6′,2″-terpyridine-4′-carboxylic acid.

Both 1D and 2D NMR data of **2**, i.e. chemical shifts, integrations, peak multiplicity, and 2D homo- and hetero-nuclear coupling experiments, suggested the existence of two (detectable) isomers in a 76/24 ratio. Thus, in the aromatic region of the ^{1}H NMR spectra of **2** (Supporting Information), two sets of resonances were

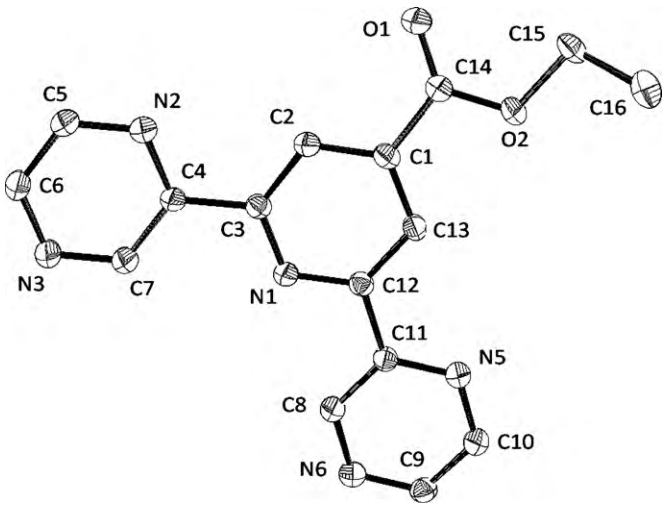

Fig. 3. ORTEP-type drawing of the crystal structure of ethyl 2,6-dipyrazin-2-ylisonicotinate, with 50% probability ellipsoids and hydrogen atoms omitted for clarity. Selected bond lengths (all ±0.002 Å) and angles (all ±0.1°): C3-N1 1.341 Å, C12-N1 1.340 Å, C2-C3 1.397 Å, C12-C13 1.400 Å, C1-C2 1.386 Å, C1-C13 1.392 Å, C1-C14 1.500 Å, C14-O1 1.208 Å, C14-O2 1.330 Å, C3-C4 1.483 Å, C12-C11 1.487 Å, N1-C3-C4 116.4°, N1-C12-C11 115.5°, C3-C4-N2 116.9°, C12-C11-N5 118.0°, N1-C3-C4-N2 179.8°, N1-C12-C11-N5 −172.3°.

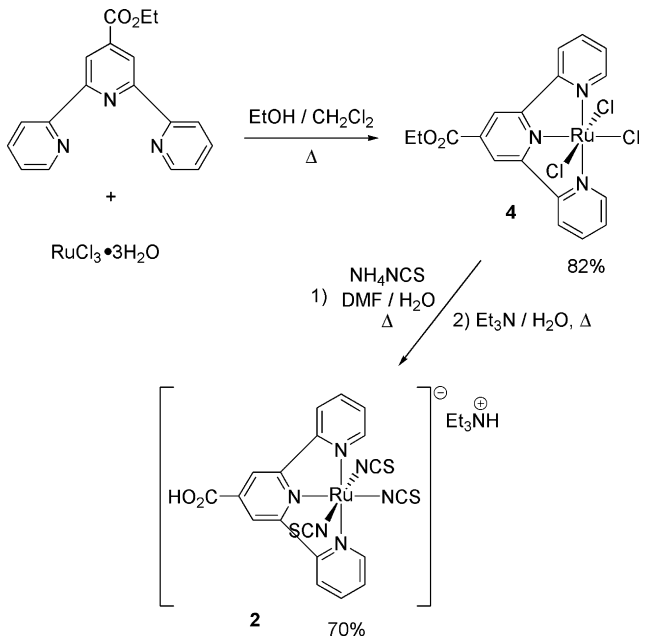

Scheme 1. Synthesis of the terpyridine-coordinated ruthenium dye **2**.

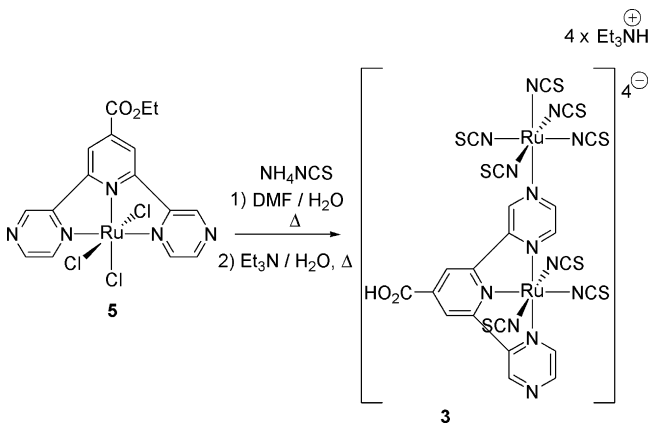

Scheme 2. Synthesis of the 2,6-dipyrazinylpyridine-coordinated ruthenium complex **3**.

observed. In particular, between δ 9.05 and 8.70 ppm, where peaks do not overlap significantly, two doublets at δ 8.99 and 8.95 ppm, for the major and minor isomers, respectively, and two singlets at δ 8.80 and 8.76 ppm, for the minor and major isomers, respectively, were recorded. The two low-field doublets correspond to the two protons *ortho* to the nitrogen atoms of the terpyridine ligand, whereas the singlets arise from the protons of the central pyridine moiety. Both the major and the minor isomers show five signals in the aromatic region, sometimes overlapping with each other, suggesting that the peripheral pyridine rings of the terpyridine ligand are magnetically equivalent; i.e. that both complexes (major and minor isomers) are symmetrical. Also, the integration ratios of the terpyridine ligand resonances and of the aliphatic peaks of Et_3NH (at δ 3.21 and 1.30 ppm), suggest that each Et_3NH cation corresponds to one ruthenium center. By taking these spectral data into consideration, we conclude that complex **2** is most probably isolated in the form of two isomers due to the ambidentate nature of its NCS ligands; that is we attribute the two different sets of NMR resonances to two linkage isomers of **2** (N-coordinated vs. S-coordinated NCS – also refer Section 3.3).

The molecular ion of **2** was detected by negative-mode ESI-TOF/MS at *m*/*z* 552.9160 (**2** requires 552.9154); a fragment corresponding to $[M–H–NCS]^-$ was also found at *m*/*z* 493.9.

We also targeted the 2,6-dipyrazinylpyridine-substituted analogue of complex **2**, to study the effect of this more electron-withdrawing ligand on the sensitizing properties of the resulting ruthenium(II) complex. The preparation of complex **5** (Scheme 2), that is, the precursor to the dipyrazinylpyridine analogue of **2**, was straightforward, following the reaction conditions utilized for parent complex **4** (Scheme 1). However, in the next step of the synthetic procedure, binuclear complex **3** (Scheme 2) was isolated instead of the anticipated dipyrazinylpyridine analogue of **2** (vide infra), along with some very minor unidentified impurities that we were unable to completely remove. Apparently, a part of the 2,6-dipyrazinylpyridine-substituted trichloride complex **5** falls apart under these conditions, affording free 2,6-dipyrazin-2-ylisonicotinic acid and the corresponding decoordinated ruthenium species; in fact, we were indeed able to isolate free 2,6-dipyrazin-2-ylisonicotinic acid from the reaction mixture, but no investigation of the fate of the resultant ruthenium species was attempted. Complex **3**, although obtained somewhat impure, was characterized by ^1H and ^{13}C NMR experiments, UV–vis and FTIR spectroscopy, as well as ESI-TOF mass spectrometry.

In the ^1H NMR spectra of **3** (Supporting Information), the integrated ratio between the aromatic (dipyrazinylpyridine) and the aliphatic (Et_3NH) resonances shows the presence of four Et_3NH counter ions per 2,6-dipyrazin-2-ylisonicotinic acid ligand, suggesting a total charge of −4 for this ruthenium complex. Moreover, eight instead of the expected four resonances in the aromatic region suggest that the two pyrazine rings of the dipyrazinylpyridine ligand are not magnetically equivalent, and, therefore, the complex is unsymmetrical. We speculate that this "desymmetrization" occurs through the attachment of a second metal center on one of the peripheral pyrazine nitrogen atoms of the ligand (complex **3**). This behavior has been *in situ* observed in the past with a similar dipyrazinylpyridine ruthenium(II) complex [48–52]; that complex showed the ability to bind Lewis acids, for instance forming Ru–Fe binuclear clusters that bear structural resemblance to the herein proposed binuclear structure.

Finally, although it has not been possible to observe the molecular tetraanion neither via ESI-TOF/MS nor via ESI/MS (Supporting Information), some of the detected fragments could very well originate from complex **3**. For example, the monoanion at *m*/*z* = 772.7612 in the negative-mode ESI-TOF spectrum could be $[M–3NCS]^-$ (requiring 772.7605). Other fragments suggest the presence of trinuclear ($[L_2Ru_3(SCN)_8]^{2-}$ with L representing the dipyrazinylisonicotinic acid ligand: *m*/*z* = 663.8375, requiring 663.8332) and mononuclear (*m*/*z* = 555.9) analogues of **3**, but these may have been formed *in situ* (as possible sampling artifacts) during the ESI-TOF experiments.

Indisputable structural assignment of complex **3** would arise from the crystallographic analysis of a single-crystal; however, it has thus far been impossible to obtain single-crystals suitable for X-ray crystallographic analysis from any of the newly synthesized complexes. To conclude, although the structure of complex **3** has not been proven beyond any doubt, the structure depicted in Scheme 2 is consistent with all existing spectroscopic data described above. Despite its accidental formation, the unusual structure of bimetallic **3** complex presents high interest from both structural and electrochemical point of view and warrants further investigation, however that extends beyond the objectives of the present study.

3.2. UV–vis and emission studies

UV–vis absorption spectra of the dyes in solution (DMF) as well as upon TiO_2 films, from transmittance and diffuse reflectance

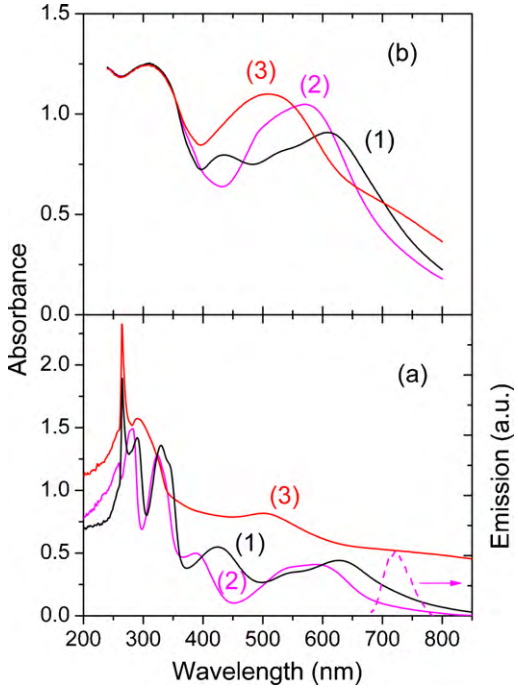

Fig. 4. Absorption spectra of dyes **1**, **2**, and **3** in DMF solution (a), and corresponding spectra of the dyes chemisorbed onto TiO_2 films (b). The emission spectrum of dye **2** (a) is also given (arbitrary units).

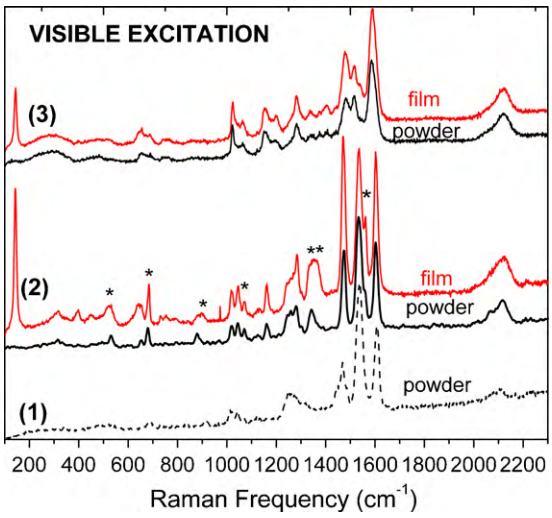

Fig. 5. Resonant Raman spectra of dyes **2** and **3** in the powder form and after sensitization of thick TiO_2 films. A Raman spectrum of black dye (**1**) is shown for comparison. The modes discussed for dye **2** are marked with a star.

experiments, respectively, are shown in Fig. 4. The absorption spectra of dye **2** are dominated by MLCT transitions with absorption maxima at 588, 535 (as a shoulder), and 390 nm. High-energy narrow bands, due to π–π^* intra ligand transitions, are shown at 327 and 280 nm. The molar extinction coefficient at 588 nm is 7640 M^{-1} cm^{-1}. Black dye (**1**), the UV–vis spectrum of which is shown for comparison, presents MLCT transitions with absorption maxima at 627, 543, and 425 nm (Table S1 in Supporting Information). Dye **3**, on the other hand, has a completely different spectrum with a broad MLCT band at 503 nm, and π–π^* transitions at 293 and 265 nm, which are similar to those of tris(bipyrazine)ruthenium(II) complexes [48,50]. A very broad absorption band at the NIR region is also observed, possibly due to the $Ru(NCS)_5$ unit. Upon TiO_2 sensitization, the wavelengths of the absorption maxima are only slightly affected. The absorption band of dye **2** keeps its shape, while for dye **3** a clear broadening is observed. This effect could be a sign of possible dye **3** agglomeration on the TiO_2 film. Finally, as can be seen in Fig. 4, dye **2** shows an approximate 40 nm blue shift of λ_{max} in comparison with black dye (**1**) [33].

The emission properties of the dyes were studied in DMF. A typical spectrum of complex **2** (presenting a maximum at 720 nm) superimposed on the corresponding absorbance curve is given in Fig. 4(a). From the intersection between the UV–vis and emission spectra [53–55], the excitation transition energy $E_{0\text{-}0}$ is determined to be 1.80 eV (690 nm). Using the absorption and emission data of black dye, the corresponding absorption threshold was estimated at about 1.49 eV.

3.3. Infrared studies

The most direct evidence regarding the coordination mode of ambidentate ligands arises from the corresponding infrared spectra. In the case of NCS ligands, the presence of absorption bands at about 2100 cm^{-1} [ν(C=N) stretching] and 780 cm^{-1} [ν(C=S) stretching] is commonly considered as a confirmation of N-coordination [56,57]. On the contrary, absorptions at about 2080 cm^{-1} [ν(C=N) stretching] and 700 cm^{-1} [ν(C=S) stretching] are suggestive of S-coordination. Another methodology that has been utilized to distinguish between N- and S-coordination modes of NCS is based on the differences in the intensity of the ν(C=N) stretching band [58,59]. The FTIR spectra of **2** were recorded in the 4000–400 cm^{-1} region (Supporting Information). The strong and relatively broad absorption observed at 2104 cm^{-1} is attributed to the characteristic ν(C=N) stretching vibration of both the N- and the S-coordinated NCS ligands (both linkage isomers of complex **2** – vide supra). Moreover, the two bands at 791 and 764 cm^{-1} [ν(C=S) stretching] can be assigned to the all-N- and all-S-coordinated isomers of ruthenium(II) complex **2**, respectively, in close agreement with the corresponding linkage isomers of black dye (**1**, Fig. 1), where the analogous stretching bands are observed at 788 and 757 cm^{-1}, respectively [59]. Finally, the band at 1693 cm^{-1} is assigned to the C=O stretching band of the protonated carboxyl group in **2** (the precursor ester moiety in complex **4** is observed at 1720 cm^{-1} – Supporting Information). Dye **3** shows similar characteristics with dyes **1** and **2**, presenting a broad C=N stretching mode at 2098 cm^{-1}, and the C=S modes at 789 and 775 cm^{-1}, due to both N- and S-coordinated NCS ligands. The carboxyl C=O stretching mode in **3** is observed at 1716 cm^{-1} (the precursor ester group in **5** resonates at 1722 cm^{-1} – Supporting Information). The rich FTIR spectra in the fingerprint region (1000–1800 cm^{-1}) for both dyes (**2** and **3**) is due to the various atomic vibrations of the terpyridine- (dye **2**) and 2,6-dipyrazinylpyridine-ligands (dye **3**). It should be also noted that the infrared spectra of dye **2** exert pronounced similarities with that of dye **1**, as expected [33]. Complementary vibrational analysis, carried out by off-resonance Raman (under NIR) and Resonance Raman (under visible excitation) scattering, is discussed in the following section.

3.4. Raman and Resonance Raman studies

Off-resonance Raman peaks of dye **2** under NIR excitation (Fig. S1, Supporting Information) could be observed neither for the dye in powder form, nor when it is adsorbed on the TiO_2 surface, due to the strong photoluminescence band recorded in the emission spectra (Fig. 4(a)). Resonant Raman spectra of dye **2** are shown in Fig. 5, both in powder form as well as when anchored on the film. The spectra are very similar to that of black dye (**1**), which we also recorded and included in the same figure for comparison purposes. The C=N frequency of the NCS ligand is

shown at 2120 cm^{-1}, with a shoulder at 2068 cm^{-1}, indicating both N- and S-type coordination to ruthenium(II), in perfect agreement with the IR analysis. The high-frequency pyridine C=C and C=N modes do not change significantly, shifted by less than 4 cm^{-1}, as expected from their rigid character. However, some remarkable differences are predominant in the range of 1100–1400 cm^{-1}, where vibrations of single C–C, C–H, and C–N modes are expected.

The most evident differences between dye **2** and black dye (**1**) are the modes emerging in the spectra at 1162 and 1340 cm^{-1}; the latter may be assigned to the combined in-plane C–H and C–C vibrations in the pyridine rings, as also observed in non-carboxylated pyridine-containing ligands such as in $Ru(terpy)_2[PF_6]_2$, and others [39,60,61]. Also, it is very interesting that low-frequency modes at 922, 694 (in-plane pyridine deformation), and 535 (out-of-plane pyridine deformation) soften to 890–900, 680, and 530 cm^{-1}, which stems from the missing carboxyl groups on the pyridine moieties of dye **2**.

Upon dye **2** sensitization of the films, notable changes in the Resonant Raman spectra are observed. First off, the TiO_2 anatase modes at low frequencies (100–650 cm^{-1}) emerge, the strongest being the 143 cm^{-1} band. Furthermore, important changes in the relative intensities of the major C=O and C=N peaks at high frequencies are observed, as well as marked variations of the C–H and C–C modes in the 1250–1350 cm^{-1} region, in agreement with the findings in other dyes [40] where such changes are attributed to surface-enhanced Raman scattering effects. New modes are also detected due to the linkage of the dye to the semiconductor (via COO^-), at 1373 cm^{-1} (symmetric stretching mode of the carbonyl groups ν_s C=O (COO^-)), and at 1560 cm^{-1} (possibly the corresponding antisymmetric mode) [62]. All the above differences, together with the absence of the protonated carboxyl group at about 1700 cm^{-1}, verify chemisorption of the dye on the semiconducting surface, most likely via bidentate chelation or bridging-type coordination [63].

The analysis of the off-resonance Raman spectrum of dye **3** (Fig. S1, Supporting Information) shows several strong lines, due to C=N related vibrations, at 1480 and 1516 cm^{-1}, as well C-N related modes at 1200 and 1282 cm^{-1}, in accordance with results on tris(bipyrazine)ruthenium(II) complexes and heteroleptic complexes with pyridine and bipyrazine [64,65]. The strong intensity of the above modes is justified by the increased number of such bonds in the pyrazine rings, and the rich spectrum in these regions due to the co-existence of one pyridine moiety. Peaks at 1150 and 1340 cm^{-1} are also observed in this case, as for dye **2**, and these are attributed to combined C–H and C–C internal ring vibrations.

The Resonant Raman spectrum of dye **3** (Fig. 5) was obtained by exciting the dye at 514 nm, very close to its MLCT transition (503 nm). Similarities with the Resonance Raman spectra in an earlier work [64,65], are pronounced both in the general pattern of Raman lines as well as their frequencies. Marked variations are observed in comparison to the spectrum obtained under NIR excitation of the dye, mainly regarding the intensity of several vibration bands. Thus, strong modes at 1034 and 1460 cm^{-1}, observed under NIR excitation, are nearly missing under visible excitation, while, on the other hand, intense modes at 1024 and 1540 cm^{-1} emerge. This is due to the excitation into the MLCT which gives rise to resonance enhancement of symmetric stretching vibrations [33,66], and selective enhancement of the pyrazine modes relative to pyridine ones [64].

Resonant Raman spectra of TiO_2 films sensitized with dye **3** do not show important differences as to the corresponding spectra of the dye in the powder form, besides the appearance of the TiO_2 modes. Sharp features, like those observed with dye **2**, were not found in this case suggesting poor dye sensitization of the film.

Table 1
HOMO–LUMO energies of Ru(II) complexes and absorption threshold values.

Sensitizer	HOMO[a] (V vs. Ag/AgCl)[b]	$E_{0\text{-}0}$[c] nm (eV)	LUMO[d] (V vs. Ag/AgCl)[b]
Dye (**2**)[e]	0.87	690 (1.80)	−0.93
Black dye (**1**)[f]	0.66	835 (1.49)	−0.83

[a] Electrochemical data.
[b] Under these conditions, the Fc/Fc^+ redox potential value was determined at +0.60 V vs. Ag/AgCl and was used as the standard reference.
[c] Derived from the spectra in Fig. 5 and Ref. [32].
[d] Calculated.
[e] In CH_3CN.
[f] In CH_3CN.

3.5. Electrochemical studies

The cyclic voltammogram (Fig. S3, Supporting Information) of dye **2** in acetonitrile, containing 0.1 M tetrabutylammonium tetraboronfluoride (TBATBF), presents a reversible wave at +0.87 V (vs. Ag/AgCl) attributed to the Ru^{3+}/Ru^{2+} redox couple as well as a reversible ligand reduction centered at −1.35 V (vs. Ag/AgCl). Under identical experimental conditions, the corresponding voltammogram of black dye (**1**) shows a reversible wave at +0.66 V (vs. Ag/AgCl) [32,33]. Using the excitation HOMO–LUMO transition energy value $E_{0\text{-}0}$ = 1.80 eV from Fig. 4, the LUMO energy level for **2** is estimated to about −0.93 V vs. Ag/AgCl (Table 1). The corresponding LUMO level in the case of black dye was estimated at approximately −0.83 V, by considering the derived $E_{0\text{-}0}$ = 1.49 eV value [32].

The LUMO levels of both dyes **1** (black dye) and **2** lie well above the TiO_2 conduction band (−0.6 V vs. Ag/AgCl [8]) permitting electron injection from the excited dye molecules into the semiconductor conduction band. Greater injection rates are expected for dye **2**, as the driving force (energetic difference between LUMO and CB) is larger than in the case of dye **1**. The corresponding HOMO levels lie below the I^-/I_3^- redox potential (+0.3 V vs. Ag/AgCl) allowing easy cation reduction for both dyes.

The corresponding CV of binuclear complex **3** was also recorded under similar experimental conditions. This complex presents an irreversible ruthenium (II)-based oxidation wave at +1.35 V (vs. Ag/AgCl), together with two quasi irreversible ligand-based reductions centered at −0.66 and −1.14 V (vs. Ag/AgCl, Fig. S3 in Supporting Information). The bridging pyrazine ligand is a well-known redox active center, being reduced at negative potentials because of its strong π-acidity and usually accommodating two reduction waves in bimetallic complexes [67]. Furthermore, the existence of only one oxidation wave in bimetallic complex **3** is indicative of poor electronic communication between the two ruthenium centers and/or low stability of the corresponding oxidized ruthenium species [68]. In the case of complex **3**, the determination of the energetic diagrams was not possible, due to both relative electrochemical irreversibility and poor fitting between the corresponding UV–vis and emission spectra (Fig. S2, Supporting Information).

3.6. Quantitative determination of dyes' adsorption

As described above, the presence of the sensitizer on the photoelectrode was qualitatively confirmed by applying Raman and UV–vis spectroscopy on the dye-sensitized titania films. A next step was then to quantify the chemisorption of the dye on the titania films; to determine the amount of the dye adsorbed, desorption experiments (carried out in $EtOH/H_2O$ NaOH solutions) were performed following standard procedures [69]. Using this approach [70], the surface density of the adsorbed dye was estimated to be 2.63×10^{-7} mol/cm^2 for dye **2**, more than 2.5 times

Table 2
Performance parameters of DSSCs based on titania films sensitized by different dyes. The surface density of adsorbed dyes is also given.

Sensitizer	J_{sc} (mA/cm^2)	V_{oc} (mV)	FF	η (%)	Dye (mol/cm^2)
Dye **2**	6.19	616	0.65	2.48	2.63×10^{-7}
Dye **3**	0.27	214	0.34	0.02	1.09×10^{-7}
Black dye (**1**)	10.23	717	0.63	4.64	4.65×10^{-8}

higher than the loading of dye **3** (1.09×10^{-7} mol/cm^2, Table 2). This difference can be attributed to the chemical structure of **3**, most probably being a binuclear complex (vide supra), that sterically inhibits its sensitization efficiency by providing much fewer dye monolayers on the TiO_2 semiconductor in comparison with dye **2**. In any case, both complexes present reasonable dye amount values in relation to other efficient dyes, recently reported in literature [71], implying that light-harvesting efficiency will not be a limiting factor for attaining high photovoltaic efficiency. Moreover, it is interesting to observe that both novel dyes are adsorbed on TiO_2 to a greater degree than black dye **1** (in qualitative agreement with the reflectance spectra of the dyes on TiO_2 substrates, Fig. 4). This result is closely related to the number of carboxylic groups that are available for adsorption in every dye; dyes **2** and **3** contain only one carboxylic group, while black dye contains three carboxylic moieties and is adsorbed through two of them [63]. A factor that could account for better adsorption in the case of dyes **2** and **3**, in relation to black dye, is the great flexibility of the dyes attached via one anchoring group on TiO_2, which would require less space, allowing more dye molecules to adsorb on the titania surface. In any case, especially concerning dye **3**, probable agglomeration on the TiO_2 substrate (previously confirmed by optical measurements) could also lead to higher loading. However, aggregation usually implies either intermolecular quenching of the excited state energy and/or reduced injection efficiency since additional layers on top of titania particles cannot inject electrons directly into the semiconductor.

3.7. Photovoltaic studies

The photovoltaic performance of the sensitized photoelectrodes was examined following their incorporation into sandwich-type liquid DSSCs. The *I–V* characteristics were then obtained under 1 sun (AM1.5) illumination (Fig. 6). The power-conversion efficiency (η) determined for the dye **2**-based cells was as high as 2.48%, with a short-circuit current (J_{sc}) of 6.19 mA/cm^2, an open-circuit potential (V_{oc}) of 616 mV, and a filling factor (FF) of 0.65. On the other hand, the corresponding efficiency for the dye **3**-based cell was extremely poor, of the order of only 0.02% (Supporting Information, Fig. S4). Additional experiments using deoxycholic acid as co-adsorbent in order to reduce agglomeration did not improve the efficiency of dye **3**, the poor value of which is obviously due to the molecular structure of the complex. Thus, it can be considered that the LUMO level lies below the CB, in part because of the added nitrogens, in part because of the appended metal, both serving to shift the redox potentials to more positive values. Comparative results performed on identical DSSCs prepared using the black dye (containing two more carboxylic acid moieties) [33] showed that the efficiency of the cells obtained from dye **2** is about the half of that attained by the black dye (Table 2). The obtained result is rather satisfactory, especially if we bear in mind that black dye is among the very few dyes that give overall energy conversion efficiency over 10% [72]. The efficiency losses arise from the lower V_{oc} (about 100 mV) and mainly due to the lower photocurrent (more than 4 mA/cm^2) gained by the dye-**2** based cell. Trying to explain the above differences, preliminary studies on the electron dynamics governing the cells constructed with the two different dyes were conducted.

Initially, the electron lifetimes were determined by performing IMVS experiments on the two cells (Fig. 7(a)). It was found that

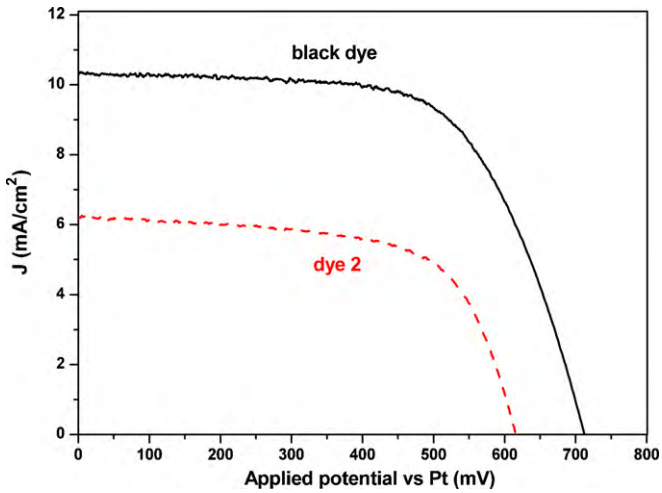

Fig. 6. *I–V* characteristics of DSSCs using TiO_2 electrodes sensitized by different dyes under illumination of 1 sun (AM 1.5).

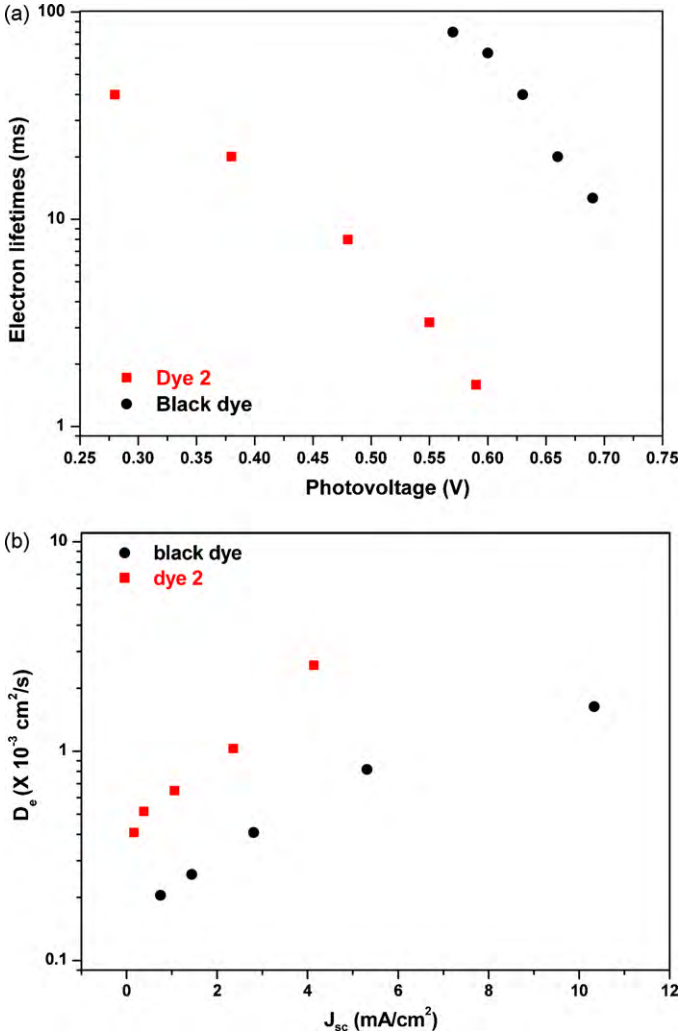

Fig. 7. (a) Electron lifetimes derived from the IMVS diagrams with varying photovoltage (with variation of the LED DC illumination power), and (b) electron diffusion coefficients derived from the IMPS diagrams with varying J_{sc}.

the black dye-based DSSCs gave much higher electron lifetimes (12.7 ms at high illumination intensities) than the ones determined for the dye **2**-based cell (only 1.56 ms at identical incident power density). These results fully confirm the differences observed at V_{oc} values, implying clearly less recombination in the case of the black dye. In terms of the two dyes structures, the greater dye coverage of dye **2** on TiO_2 (in relation to black dye) implies higher protection from I_3^- ions, which scavenge the surface electrons when closely surrounding the TiO_2 particles. Thus, the higher recombination observed with dye **2** probably suggests increased recombination with dye cations (and not I_3^-). This back-reaction is frequently considered important under open-circuit conditions in a DSSC, decreasing V_{oc} values [73]. Nevertheless, differences in the conduction band edges of TiO_2 upon adsorption of the two dyes cannot be excluded as a possible reason to explain the V_{oc} differences, due to different sensitizer adsorption geometry inducing dipolar fields of different magnitude and orientation at the surface of the semiconductor particle [74]. In this context, we have performed electrochemical impedance (EIS) measurements (Fig. S5, Supporting Information) in order to estimate the chemical capacitance of the semiconductor for the two cells [75]. It was found that the at the same film capacitance, the dye **2**-based cell presents a higher voltage (about 250 mV) than the one corresponding to black dye, implying that the adsorption of dye **2** on the semiconductor shifts the TiO_2 conduction band towards more negative potentials [76]. However, this shift is not accompanied by an enhancement of V_{oc} due to the dramatic increase of the recombination rate (that finally diminishes the overall V_{oc} values by about 100 mV).

On the other hand, significant differences were observed on the photocurrent delivered by the two cells. The J_{sc} in a DSSC depends on the light harvesting of the photoelectrode, the injection efficiency of the electrons from the dye onto the semiconductor, and, lastly, the collection efficiency of the electrons at the back contact. The light-harvesting ability of dye **2** is significantly lower than that of dye **1** above 600 nm (Fig. 4(b)), however this change cannot solely account for the large J_{sc} differences. Differences in charge injection efficiencies (concerning the driving force for electrons injection) are difficult to be evaluated since the LUMO of dye **2** is higher than that of dye **1** (Table 1), but coincidently the conduction band edge of TiO_2 is also higher upon adsorption of dye **2** in comparison with dye **1**. Thus, the only probability that remains to justify the observed J_{sc} differences is the higher charge collection efficiency in the case of black dye (**1**). This parameter is usually estimated by the measurement of the diffusion length (L_n) at short-circuit, using the formula $L_n = \sqrt{D_e \times \tau_n}$ [77]. Despite the fact that the real value of L_n could not be accurately measured here [78], a rough estimation of the diffusion length could be realized for comparison reasons only. Thus, using the above equation, the diffusion lengths were determined for the two dyes, being about 45 μm for black dye and only 20 μm for dye **2** at strong illumination conditions (to mimic the *I–V* curves under 1 sun illumination). It was then found that black dye (**1**) had a value of L_n more than double that of dye **2**, while we must highlight the fact that the diffusion length for dye **2** did not overcome the film thickness (being 22 μm), implying that electrons would be lost during their diffusion towards the rear contact. The above preliminary findings seem to accurately explain the J_{sc} differences observed between the two dyes. These results are in agreement with other literature reports, which proposed that dyes with a higher number of carboxylic groups (such as black dye in the present case), can affect the dynamics of recombination of the charge-separated state of the dye/TiO_2 moieties in a positive way (in relation to monocarboxylate-containing complexes like dyes **2** and **3**) [79]. Similar results have been also resolved by other groups studying analogous homoleptic Ru(II) complexes [80,81].

4. Conclusions

Two novel ruthenium(II) dyes, coordinated with terpyridine- or 2,6-dipyrazinylpyridine-based ligands, have been synthesized and characterized. The structure of the terpyridine-bearing complex resembles that of black dye; on the other hand, the spectral data of the 2,6-dipyrazinylpyridine-coordinated complex suggest an unexpected binuclear structure in which one of the peripheral pyrazine nitrogen atoms of the ligand is attached to a second ruthenium(II) center. The Ru^{2+}/Ru^{3+} oxidation potential of the terpyridine-coordinated dye in acetonitrile was measured at +0.87 V (vs. Ag/AgCl); this is about 200 mV higher than the oxidation potential of black dye. Both new dyes were found to adsorb on TiO_2 films to a higher extent than black dye. Furthermore, the photo-electrochemical properties of both dyes were investigated; interestingly, solar cells obtained from the terpyridine-coordinated dye show power-conversion efficiencies which are more than half of those attained by the black dye. The electron dynamics in cells containing the new terpyridine dye were also studied and compared to that of black dye.

Acknowledgments

The authors acknowledge financial support from the General Secretariat for Research and Technology (GSRT-Greece) through PENED project 03ED 118/2005. T. Stergiopoulos thanks the Greek State Scholarships Foundation (IKY) for a fellowship. Helpful assistance by Dr. L. Leontiadis in obtaining the ESI-MS spectra is also gratefully acknowledged.

Appendix A. Supplementary data

Supplementary data associated with this article can be found, in the online version, at doi:10.1016/j.jphotochem.2010.06.001.

References

[1] Energy and Environment Report 2008, European Environment Agency, Office for Official Publications of the European Communities, Copenhagen, 2008.
[2] N. Armaroli, V. Balzani, The future of energy supply: challenges and opportunities, Angew. Chem. Int. Ed. 46 (2007) 52–66.
[3] R.E. Blankenship (Ed.), Molecular Mechanisms of Photosynhtesis, Blackwell Science, Oxford, 2002.
[4] The journal "Inorganic Chemistry" has recently presented a forum on solar and renewable energy: Inorg. Chem. 44 (2005) 6799–7260.
[5] M. Grätzel, Photoelectrochemical cells, Nature 414 (2001) 338–344.
[6] L.M. Goncalves, V. de Zea Bermudez, H.A. Ribeiro, A.M. Mendes, Dye-sensitized solar cells: a safe bet for the future, Energy Environ. Sci. 1 (2008) 655–667.
[7] The journal "Coordination Chemistry Reviews" has published a special issue on DSSCs: Coord. Chem. Rev. 248 (2004) 1161–1530. For some representative review articles on DSSCs the reader may consult Refs. [8–14].
[8] A. Hagfeldt, M. Grätzel, Light-induced redox reactions in nanocrystalline systems, Chem. Rev. 95 (1995) 49–68.
[9] R. Argazzi, N.Y.M. Iha, H. Zabri, F. Odobel, C.A. Bignozzi, Design of molecular dyes for application in photoelectrochemical and electrochromic devices based on nanocrystalline metal oxide semiconductors, Coord. Chem. Rev. 248 (2004) 1299–1316.
[10] M.K. Nazeeruddin, S.M. Zakeeruddin, J.-J. Lagref, P. Liska, P. Comte, C. Barolo, G. Viscardi, K. Schenk, M. Graetzel, Stepwise assembly of amphiphilic ruthenium sensitizers and their applications in dye-sensitized solar cell, Coord. Chem. Rev. 248 (2004) 1317–1328.
[11] A.S. Polo, M.K. Itokazu, N.Y.M. Iha, Metal complex sensitizers in dye-sensitized solar cells, Coord. Chem. Rev. 248 (2004) 1343–1361.
[12] G.J. Meyer, Molecular approaches to solar energy conversion with coordination compounds anchored to semiconductor surfaces, Inorg. Chem. 44 (2005) 6852–6864.
[13] N. Robertson, Optimizing dyes for dye-sensitized solar cells, Angew. Chem. Int. Ed. 45 (2006) 2338–2345.
[14] P. Xie, F. Guo, Molecular engineering of ruthenium sensitizers in dye-sensitized solar cells, Curr. Org. Chem. 11 (2007) 1272–1286.
[15] This type of cell was reported for the first time in 1991: B. O'Regan, M. Grätzel, A low-cost, high-efficiency solar cell based on dye-sensitized colloidal TiO_2 films, Nature 353 (1991) 737–740.

[16] M.R. Wasielewski, Photoinduced electron transfer in supramolecular systems for artificial photosynthesis, Chem. Rev. 92 (1992) 435–461.
[17] J.L. Bredas, D. Beljionne, V. Coropceanu, J. Cornil, Charge-transfer and energy-transfer processes in π-conjugated oligomers and polymers: a molecular picture, Chem. Rev. 104 (2004) 4971–5003.
[18] K. Hara, T. Sato, R. Katoh, A. Furube, Y. Ohga, A. Shinpo, S. Suga, K. Sayama, H. Sugihara, H. Arakawa, Molecular design of coumarin dyes for efficient dye-sensitized solar cells, J. Phys. Chem. B 107 (2003) 597–606.
[19] K. Hara, Z.-S. Wang, T. Sato, A. Furube, R. Katoh, H. Sugihara, Y. Dan-oh, C. Kasada, A. Shinpo, S. Suga, Oligothiophene-containing coumarin dyes for efficient dye-sensitized solar cells, J. Phys. Chem. B 109 (2005) 15476–15482.
[20] J.-H. Yum, P. Walter, S. Huber, D. Rentsch, T. Geier, F. Nuesch, F. De Angelis, M. Grätzel, M.K. Nazeeruddin, Efficient far red sensitization of nanocrystalline TiO_2 films by an unsymmetrical squaraine dye, J. Am. Chem. Soc. 129 (2007) 10320–10321.
[21] Z.-S. Wang, Y. Cui, K. Hara, Y. Dan-oh, C. Kasada, A. Shinpo, A high-light-harvesting-efficiency coumarin dye for stable dye-sensitized solar cells, Adv. Mater. 19 (2007) 1138–1141.
[22] W.H. Wowie, F. Claeyssens, H. Miura, L.M. Peter, Characterization of solid-state dye-sensitized solar cells utilizing high absorption coefficient metal-free organic dyes, J. Am. Chem. Soc. 130 (2008) 1367–1375.
[23] Z.-S. Wang, N. Koumura, Y. Cui, M. Takahashi, H. Sekiguchi, A. Mori, T. Kubo, A. Furube, K. Hara, Hexylthiophene-functionalized carbazole dyes for efficient molecular photovoltaics: tuning of solar-cell performance by structural modification, Chem. Mater. 20 (2008) 3993–4003.
[24] J.-J. Cid, M. Garcia-Iglesias, J.-H. Yum, A. Forneli, J. Albero, E. Martinez-Ferrero, P. Vazquez, M. Grätzel, M.K. Nazeeruddin, E. Palomares, T. Torres, Structure–function relationships in unsymmetrical zinc phthalocyanines for dye-sensitized solar cells, Chem. Eur. J. 15 (2009) 5130–5137.
[25] F. Gao, Y. Wang, D. Shi, J. Zhang, M. Wang, X. Jing, R. Humphry-Baker, P. Wang, S.M. Zakeeruddin, M. Grätzel, Enhance the optical absorptivity of nanocrystalline TiO_2 film with high molar extinction coefficient ruthenium sensitizers for high performance dye-sensitized solar cells, J. Am. Chem. Soc. 130 (2008) 10720–10728.
[26] F. Gao, Y. Wang, J. Zhang, D. Shi, M. Wang, R. Humphry-Baker, P. Wang, S.M. Zakeeruddin, M. Grätzel, A new heteroleptic ruthenium sensitizer enhances the absorptivity of mesoporous titania film for a high efficiency dye-sensitized solar cell, Chem. Commun. (2008) 2635–2637.
[27] D. Shi, N. Pootrakulchote, R. Li, J. Guo, Y. Wang, S.M. Zakeeruddin, M. Grätzel, P. Wang, New efficiency records for stable dye-sensitized solar cells with low-volatility and ionic liquid electrolytes, J. Phys. Chem. C 112 (2008) 17046–17050.
[28] B. Liu, W. Zhu, W. Wu, K.M. Ri, H. Tian, Hybridized ruthenium(II) complexes with high molar extinction coefficient unit: effect of energy band and adsorption on photovoltatic performances, J. Photochem. Photobiol. A: Chem. 194 (2008) 268–274.
[29] F. Gao, Y. Cheng, Q. Yu, S. Liu, D. Shi, Y. Li, P. Wang, Conjugation of selenophene with bipyridine for a high molar extinction coefficient sensitizer in dye-sensitized solar cells, Inorg. Chem. 48 (2009) 2664–2669.
[30] M.K. Nazeeruddin, A. Kay, I. Rodicio, R. Humphry-Baker, E. Muller, P. Liska, N. Vlachopoulos, M. Grätzel, Conversion of light to electricity by cis-X_2Bis(2,2′-bipyridyl-4,4′-dicarboxylate)ruthenium(II) charge-transfer sensitizers (X = Cl–, Br–, I–, CN–, and SCN–) on nanocrystalline TiO_2 electrodes, J. Am. Chem. Soc. 115 (1993) 6382–6390.
[31] M.K. Nazeeruddin, F. De Angelis, S. Fantacci, A. Selloni, G. Viscardi, P. Liska, S. Ito, B. Takeru, M. Grätzel, Combined experimental and DFT-TDDFT computational study of photoelectrochemical cell ruthenium sensitizers, J. Am. Chem. Soc. 127 (2005) 16835–16847.
[32] M.K. Nazeeruddin, P. Pechy, M. Grätzel, Efficient panchromatic sensitization of nanocrystalline TiO_2 films by a black dye based on a trithiocyanato–ruthenium complex, Chem. Commun. (1997) 1705–1706.
[33] M.K. Nazeeruddin, P. Pechy, T. Renouard, S.M. Zakeeruddin, R. Humphry-Baker, P. Comte, P. Liska, L. Cevey, E. Costa, V. Shklover, L. Spiccia, G.B. Deacon, C.A. Bignozzi, M. Grätzel, Engineering of efficient panchromatic sensitizers for nanocrystalline TiO_2-based solar cells, J. Am. Chem. Soc. 123 (2001) 1613–1624.
[34] S.M. Zakeeruddin, M.K. Nazeeruddin, R. Humphry-Baker, P. Pechy, P. Quagliotto, C. Barolo, G. Viscardi, M. Grätzel, Design, synthesis, and application of amphiphilic ruthenium polypyridyl photosensitizers in solar cells based on nanocrystalline TiO_2 films, Langmuir 18 (2002) 952–954.
[35] Y. Cao, Y. Bai, Q. Yu, Y. Cheng, S. Liu, D. Shi, F. Gao, P. Wang, Dye-sensitized solar cells with a high absorptivity ruthenium sensitizer featuring a 2-(hexylthio)thiophene conjugated bipyridine, J. Phys. Chem. C 113 (2009) 6290–6297.
[36] C.A. Mitsopoulou, I. Veroni, A.I. Philippopoulos, P. Falaras, Synthesis, characterization and sensitization properties of two novel mono and bis carboxyl-dipyrido-phenazine ruthenium(II) charge transfer complexes, J. Photochem. Photobiol. A: Chem. 191 (2007) 6–12.
[37] E. Chatzivasiloglou, T. Stergiopoulos, A.G. Kontos, N. Alexis, M. Prodromidis, P. Falaras, The influence of the metal cation and the filler on the performance of dye-sensitized solar cells using polymer-gel redox electrolytes, J. Photochem. Photobiol. A: Chem. 192 (2007) 49–55.
[38] A. Chicov, S.P. Albu, R. Hahn, D. Kim, T. Stergiopoulos, J. Kunze, C.A. Schiller, P. Falaras, P. Schmuki, TiO_2 nanotubes in dye-sensitized solar cells: critical factors for the conversion efficiency, Chem. Asian J. 4 (2009) 520–525.
[39] G. Konti, E. Chatzivasiloglou, V. Likodimos, G. Kantonis, A.G. Kontos, A.I. Philippopoulos, P. Falaras, Influence of pyridine ligand nature and the corresponding ruthenium(II) dye molecular structure on the performance of dye-sensitized solar cells, Photochem. Photobiol. Sci. 8 (2009) 726–732.
[40] V. Likodimos, T. Stergiopoulos, P. Falaras, R. Harikisun, J. Desilvestro, G. Tulloch, Prolonged light and thermal stress effects on industrial dye-sensitized solar cells: a micro-Raman investigation on the long-term stability of aged cells, J. Phys. Chem. C 113 (2009) 9412–9422.
[41] R.-A. Fallahpour, Carboxylate derivatives of oligopyridines, Synthesis (2000) 1138–1142.
[42] J. Husson, M. Beley, G. Kirsch, A novel pathway for the synthesis of a carboxylic acid-functionalised Ru(II) terpyridine complex, Tetrahedron Lett. 44 (2003) 1767–1770.
[43] E.C. Constable, E.L. Dunphy, C.E. Housecroft, M. Neuburger, S. Schaffner, F. Schaper, S.R. Batten, Expanded ligands: bis(2,2′:6′,2″-terpyridine carboxylic acid) ruthenium(II) complexes as metallosupramolecular analogues of dicarboxylic acids, Dalton Trans. (2007) 4323–4332.
[44] H. Wolpher, S. Sinha, J. Pan, A. Johansson, M.J. Lundqvist, P. Persson, R. Lomoth, J. Bergquist, L. Sun, V. Sundstrom, B. Akermark, T. Polivka, Synthesis and electron transfer studies of ruthenium-terpyridine-based dyads attached to nanostructured TiO_2, Inorg. Chem. 46 (2007) 638–651.
[45] V. Duprez, M. Biancardo, F.C. Krebs, Characterisation and application of new carboxylic acid-functionalised ruthenium complexes as dye-sensitisers for solar cells, Sol. Energy Mater. Sol. Cell 91 (2007) 230–237.
[46] M.W. Cooke, P. Tremblay, G.S. Hanan, Carboxy-derived $(tpy)_2Ru^{2+}$ complexes as sub-units in supramolecular architectures: the solubilized ligand 4′-(4-carboxyphenyl)-4,4″-di-(tert-butyl)tpy and its homoleptic Ru(II) complex, Inorg. Chim. Acta 361 (2008) 2259–2269.
[47] V.W. Manner, A.G. DiPasquale, J.M. Mayer, Facile concerted proton-electron transfers in a ruthenium terpyridine-4′-carboxylate complex with a long distance between the redox and basic sites, J. Am. Chem. Soc. 130 (2008) 7210–7211.
[48] R. Liegghio, P.G. Potvin, A.B.P. Lever, 2,6-Dipyrazinylpyridines and their ruthenium(II) complexes: a new polynucleating ligand family, Inorg. Chem. 40 (2001) 5485–5486.
[49] H.E. Toma, A.B.P. Lever, Spectroscopic and kinetic studies on a series of di- to heptanuclear tris(bipyrazine)ruthenium(II)–pentacyanoferrate(II) complexes in aqueous solution, Inorg. Chem. 25 (1986) 176–181.
[50] H.E. Toma, P.R. Auburn, E.S. Dodsworth, M.N. Golovin, A.B.P. Lever, Binding of pentaammineruthenium(II) residues to the tris(bipyrazine)ruthenium(II) cation, Inorg. Chem. 26 (1987) 4257–4263.
[51] H.E. Toma, P.S. Santos, A.B.P. Lever, Resonance Raman spectra of the heptanuclear $[Ru(bpz)_3\{Ru(NH_3)_5\}_6]^{14+}$ complex. Excitation profiles for three overlapping metal-to-ligand charge-transfer bands, Inorg. Chem. 27 (1988) 3850–3853.
[52] Y. Baran, Kinetics of formation, dissociation and equilibrium constants of pentacyanoaquoruthenate(II) with heterocycles, Trans. Met. Chem. 25 (2000) 41–44.
[53] X. Li, K. Hou, X. Duan, F. Li, C. Huang, Ruthenium(II) complex based on 4,4′-di(*p*-methylphenyl)-2,2′-bipyridine: synthesis and photoelectrochemical properties, Inorg. Chem. Commun. 9 (2006) 394–396.
[54] F. Matar, T.H. Ghaddar, K. Walley, T. DosSantos, J.R. Durrant, B. O'Regan, A new ruthenium polypyridyl dye, TG6, whose performance in dye-sensitized solar cells is surprisingly close to that of N719, the 'dye to beat' for 17 years, J. Mater. Chem. 18 (2008) 4246–4253.
[55] K. Chen, Y.H. Hong, Y. Chi, W.H. Liu, B.S. Chen, P.-T. Chou, Strategic design and synthesis of novel tridentate bipyridine pyrazolate coupled Ru(II) complexes to achieve superior solar conversion efficiency, J. Mater. Chem. 19 (2009) 5329–5335.
[56] P. Maruthamuthu, S. Anandan, Synthesis, characterization and photoconversion study of [Ru(II)(dcbpy)(terpy)Cl]Cl·3H_2O, [Ru(II)(dcbpy)(terpy)SCN]SCN·3H_2O and [Ru(II)(dcbpy)(terpy)CN]CN·3H_2O systems, Sol. Energy Mater. Sol. Cell 59 (1999) 199–209.
[57] K. Chryssou, T. Stergiopoulos, P. Falaras, Synthesis and spectroscopic properties of a new bipyridine-bipyrazoyl(pyridine)-thiocyanato-ruthenium(II) complex, Polyhedron 21 (2002) 2773–2781.
[58] L.A. Epps, L.G. Marzilli, Preparation of a mixed N-bonded-S-bonded trans-dithiocyanato complex. The three isomers of tetraphenylarsonium trans-(dithiocyanato)bis(dimethylglyoximato)cobaltate(III), Inorg. Chem. 12 (1973) 1514–1517.
[59] M.K. Nazeeruddin, M. Grätzel, Separation of linkage isomers of trithiocyanato (4,4′,4″-tricarboxy-2,2′,6,2″-terpyridine)ruthenium(II) by pH-titration method and their application in nanocrystalline TiO_2-based solar cells, J. Photochem. Photobiol. A: Chem. 145 (2001) 79–86.
[60] P.W. Hansen, P.E.W. Jensen, Vibrational studies on bis-terpyridine-ruthenium(II) complexes, Spectrochim. Acta 50A (1994) 169–183.
[61] M.C. Bernard, H. Cachet, P. Falaras, A. Hugot-Le Goff, M. Kalbac, I. Lukes, N.T. Oanh, T. Stergiopoulos, I. Arabatzis, Sensitization of TiO_2 by polypyridine dyes, J. Electrochem. Soc. 150 (2003) E155–E164.
[62] C. Perez Leon, L. Kador, B. Peng, M. Thelakkat, Influence of the solvent on the surface-enhanced Raman spectra of ruthenium(II) bipyridyl complexes, J. Phys. Chem. B 109 (2005) 5783–5789.
[63] C. Bauer, G. Boschloo, E. Mukhtar, A. Hagfeldt, Interfacial electron-transfer dynamics in Ru(tcterpy)$(NCS)_3$-sensitized TiO_2 nanocrystalline solar cells, J. Phys. Chem. B 106 (2002) 12693–12704.
[64] G.D. Danzer, J.R. Kincaid, Resonance Raman spectra of homoleptic and heteroleptic complexes of ruthenium(II) with bipyridine and bipyrazine

in the ground and 3MLCT excited states, J. Phys. Chem. 94 (1990), 3976-3980.
[65] G.D. Danzer, J.R. Kincaid, Resonance Raman spectra of $Ru(bpz)_3^{2+}$ in aqueous sulfuric acid solutions, J. Raman Spectr. 23 (1992) 681–689.
[66] C.P. Leon, L. Kador, B. Peng, M. Thelakkat, Characterization of the adsorption of Ru-bpy dyes on mesoporous TiO_2 films with UV–Vis, Raman, and FTIR spectroscopies, J. Phys. Chem. B 110 (2006) 8723–8730.
[67] S.H. Wadman, R.W.A. Havenith, F. Hartl, M. Lutz, A.L. Spek, G.P.M. van Klink, G. van Koten, Redox chemistry and electronic properties of 2,3,5,6-tetrakis(2-pyridyl)pyrazine-bridged diruthenium complexes controlled by N,C,N′-biscyclometalated ligands, Inorg. Chem. 48 (2009) 5685–5696.
[68] Y. Lin, J. Yuan, M. Hu, J. Cheng, J. Yin, S. Jin, S.H. Liu, Syntheses and properties of binuclear ruthenium vinyl complexes with dithienylethene units as multifunction switches, Organometallics 28 (2009) 6402–6409.
[69] T. Stergiopoulos, A. Ghicov, V. Likodimos, D.S. Tsoukleris, J. Kunze, P. Schmuki, P. Falaras, Dye-sensitized solar cells based on thick highly ordered TiO_2 nanotubes produced by controlled anodic oxidation in non-aqueous electrolytic media, Nanotechnology 19 (2008) 235602.
[70] T. Edvinsson, C. Li, N. Pschirer, J. Schoneboom, F. Eickemeyer, R. Sens, G. Boschloo, A. Herrmann, K. Mullen, A. Hagfeldt, Intramolecular charge-transfer tuning of perylenes: spectroscopic features and performance in dye-sensitized solar cells, J. Phys. Chem. C 111 (2007) 15137–15140.
[71] W.-H. Liu, I.-C. Wu, C.-H. Lai, P.-T. Chou, Y.-T. Li, C.-L. Chen, Y.-Y. Hsu, Y. Chi, Simple organic molecules bearing a 3,4-ethylenedioxythiophene linker for efficient dye-sensitized solar cells, Chem. Commun. (2008) 5152–5154.
[72] Y. Chiba, A. Islam, Y. Watanabe, R. Komiya, N. Koide, L. Han, Dye-sensitized solar cells with conversion efficiency of 11.1%, Jpn. J. Appl. Phys. 45 (2006) L638–L640.
[73] J.N. Clifford, E. Palomares, M.K. Nazeeruddin, M. Grätzel, J. Nelson, X. Li, N.J. Long, J.R. Durrant, Molecular control of recombination dynamics in dye-sensitized nanocrystalline TiO_2 films: free energy vs distance dependence, J. Am. Chem. Soc. 126 (2004) 5225–5233.
[74] F. De Angelis, S. Fantacci, A. Selloni, M. Grätzel, M.K. Nazeeruddin, Influence of the sensitizer adsorption mode on the open-circuit potential of dye-sensitized solar cells, Nano Lett. 7 (2007) 3189–3195.
[75] Z.P. Zhang, S.M. Zakeeruddin, B.C. O'Regan, R. Humphry-Baker, M. Grätzel, Influence of 4-guanidinobutyric acid as coadsorbent in reducing recombination in dye-sensitized solar cells, J. Phys. Chem. B 109 (2005) 21818–21824.
[76] P. Chen, J.-H. Yum, F. De Angelis, E. Mosconi, S. Fantacci, S.-J. Moon, R. Humphry-Baker, J. Ko, M.K. Nazeeruddin, M. Grätzel, High open-circuit voltage solid-state dye-sensitized solar cells with organic dye, Nano Lett. 9 (2009) 2487–2492.
[77] L.M. Peter, Dye-sensitized nanocrystalline solar cells, Phys. Chem. Chem. Phys. 9 (2007) 2630–2642.
[78] P.R.F. Barnes, L. Liu, X. Li, A.Y. Anderson, H. Kisserwan, T.H. Ghaddar, J.R. Durrant, B.C. O'Regan, Re-evaluation of recombination losses in dye-sensitized cells: the failure of dynamic relaxation methods to correctly predict diffusion length in nanoporous photoelectrodes, Nano Lett. 9 (2009) 3532–3538.
[79] A. Fillinger, B.A. Parkinson, The adsorption behavior of a ruthenium-based sensitizing dye to nanocrystalline TiO_2 coverage effects on the external and internal sensitization quantum yields, J. Electrochem. Soc. 146 (1999) 4559–4564.
[80] K. Kilsa, E.I. Mayo, B.S. Brunschwig, H.B. Gray, N.S. Lewis, J.R. Winkler, Anchoring group and auxiliary ligand effects on the binding of ruthenium complexes to nanocrystalline TiO_2 photoelectrodes, J. Phys. Chem. B 108 (2004) 15640–15651.
[81] K. Hara, H. Sugihara, L.P. Singh, A. Islam, R. Katoh, M. Yanagida, K. Sayama, S. Murata, H. Arakawa, New Ru(II) phenanthroline complex photosensitizers having different number of carboxyl groups for dye-sensitized solar cells, J. Photochem. Photobiol. A: Chem. 145 (2001) 117–122.